ISSN 1330-3651 (Print), ISSN1848-6339 (Online)
Received: 19 April 2025; Accepted: 20 November 2025

https://doi.org/10.17559/TV-20250419002609
Original scientific paper

Exposure to Electromagnetic Radiation from a 4G Smart Helmet

Vladimir STANKOVIĆ*, Dejan JOVANOVIĆ, Anđela JEVTIĆ, Miomir RAOS, Dragana ŽIVALJEVIĆ

Abstract: This paper discusses the impact of electromagnetic radiation from a smart 4G (fourth-generation mobile network) helmet on human head tissues and organs. The research was conducted at a 4G mobile network frequency of 2,6 GHz. The software used for creating 3D numerical models of the head, helmet, and 4G antenna is based on the Finite Integration Technique. The head model comprises homogeneous, isotropic domains corresponding to tissues and organs, designated by electromagnetic properties specific to the assigned radiation frequency. The helmet model was created based on the dimensions of a real sample and the corresponding specifications of the material from which it was made. The simulation results show increased values of electric field intensity and SAR (Specific Absorption Rate) in tissues directly beneath the 4G antenna of the smart helmet. The obtained results serve as a basis for future research on the impact of electromagnetic field from 4G helmets on human health.

Keywords: biological tissue; electric field; helmet; numerical models; specific absorption rate

1 INTRODUCTION

In recent times, various wireless devices are being used daily across all aspects of human life. As wireless devices become increasingly popular and widely available, more and more people will have one or more devices on their body. This presents a challenge for researchers to study the ways in which these devices are used, as well as the advantages and disadvantages of their use [1].

Owing to their complexity and wide applicability, wireless devices, such as smart watches, wrist bands, smart sunglasses, smart jewelry, electronic clothing, skin patches, etc. are used in fitness and healthcare. In addition to increasing the quality of personal life, wearable wireless devices are also used to provide various services, such as positioning and navigation, banking, physical and mental health monitoring, sports analytics, etc. [2].

In [3], a smart hazard warning system was developed, based on a helmet that provides visual and tactile warnings to workers and operators in surface mines.

To enhance work processes, a range of wireless communication devices for employees have been developed. Consequently, to make the work of employees in specific industries more efficient and transparent while maintaining all safety characteristics, the connection of protective helmets and wireless communication systems has been enabled. The so-called "smart helmet" has found extensive application in the energy sector, railways, steel industry, ports, various types of inspections, remote operations, maintenance, rescue, disaster assistance, firefighting, emergency response, and so on [4, 5]. Smart protective helmets typically provide high-level protection, preventing workers from head impacts, punctures, and other injuries. They can also detect whether workers are wearing them and issue a warning as a reminder.

Some studies examined the application of smart helmets in industry, in first responder applications, and in health tracking [6]. In the construction industry, smart helmets can be used for health and safety control through monitoring of the work environment or workers' physiological signals [7].

For first responder teams, a smart helmet can assist in detecting injuries such as bone fractures [8].

One study [9] presented the possibility of integrating artificial intelligence technology with smart helmets to enhance worker safety.

Smart protective helmets usually contain built-in wireless communication modules, allowing them to communicate with other devices, such as smartphones or computers, via mobile networks, Wi-Fi, or Bluetooth [4]. The smart helmet uses a new generation of high-speed processors, integrates HD video and audio, 4G, 3G, and Wi-Fi wireless communication, positioning, storage, alarms, multiple sensors, and physical protection. It can facilitate real-time audio and video calls, real-time video monitoring, and GPS positioning. Fig. 1 shows an example of a 4G smart helmet and one of its applications.

A person wearing a 4G smart helmet can initiate a call with one button and communicate with the dispatch center. The dispatcher can also initiate a call at any time and simultaneously capture images displayed from multiple 4G smart helmets [5, 10, 11]. The smart helmet can use frequencies from LTE-FDD, WCDMA, TD-SCDMA, and GSM bands for wireless communication [4, 5, 12].

Despite all the advantages offered by the 4G helmet, the fact remains that the core of the helmet's communication system is the 4G antenna, which emits electromagnetic radiation adjacent to the wearer's head. Therefore, it is of interest to analyze the electromagnetic radiation of the smart 4G helmet and the impact of radiation on its wearers. Some studies have considered various design solutions for antennas for helmets and electromagnetic radiation for simple phantom models [13-17].

a) b)

Figure 1 a) 4G smart helmet [3], b) Practical application of a 4G smart helmet (property of the author)

Numerical simulations represent a suitable tool for examining the distribution of electromagnetic field in human tissues and organs [18, 19]. The impact of the electromagnetic field originating from a 4G smart helmet antenna on the human head can be assessed through the values obtained for the electric field and SAR (Specific Absorption Rate).

Accordingly, realistic 3D human head and smart 4G helmet models have been developed, providing reliable results for values of the penetrating electromagnetic field originating from the smart helmet's 4G antenna. Computer Simulation Technology (CST) software package was utilized for numerical simulation of electric field values and SAR at a frequency of 2,6 GHz [20]. The impact of electromagnetic radiation depends on the composition, morphology, and dimensions of biological tissues and organs, so they must be described with adequate electromagnetic properties for a specific frequency [19, 21]. The values of the penetrated electric field and SAR will be compared with the permitted values from the Regulation on exposure limits to non-ionizing radiation, Official Gazette of the Republic of Serbia [22] and an IEEE Standard [23].

2 NUMERICAL METHOD AND MODELING

To conduct the research, a 3D numerical model was designed to represent the human head, the helmet, and the communication system. The accuracy of the results is dependent on how closely the models match the composition and dimensions of the actual helmet and communication system, as well as the tissues and organs of the human head. Each individual model had to go through several phases, including shape definition, fitting of the components, proper sizing, and positioning in space. The final phase involved assembling a unified 3D model, defining the materials, representing them with appropriate electromagnetic properties, and creating a unified mesh.

By scanning the human head using computed tomography, the exact placement of tissues and organs was determined. For an accurate simulation process of electromagnetic wave propagation, boundary conditions at the interface between two layers must be correctly defined [24]. A hexahedral mesh type was used in the simulation process.

A fine mesh can result in high memory requirements and increased simulation time. Establishing a trade-off between computation time and solution accuracy is achieved through convergence analyses, which identify the minimum grid resolution required to provide acceptable numerical accuracy.

In the present study, the computational model comprises approximately 46 million mesh elements. A discrete port is utilized to excite the mobile phone antenna, which serves as the source of the radiated electromagnetic (EM) waves. The excitation signal is time-dependent and is represented by a Gaussian-modulated sinusoidal pulse.

The simulation of the communication process of the 4G smart helmet, as well as the analysis of electric field intensity and SAR, was carried out using CST Studio Suite computer simulation software [20].

2.1 Numerical Model of the Human Head

For the purpose of analyzing the distribution of the electric field and SAR from the 4G smart helmet within the human head, a model of an adult human head was created (Fig. 2). The shape, composition, and dimensions of the numerical model match the actual properties of an average adult human head [25]. The cross-section of the numerical head model, including multiple tissues and organs, is shown in Fig. 3.

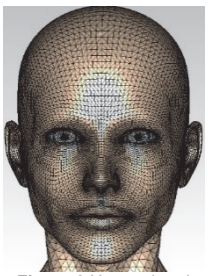

Figure 2 Human head

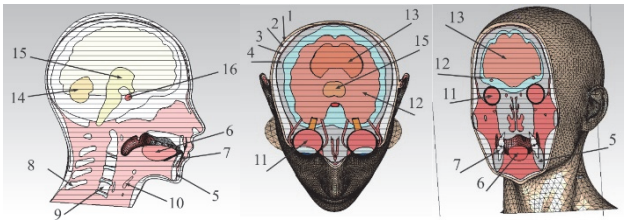

Figure 3 Human head cross-sections with the corresponding tissues and organs: 1 - skin; 2 - adipose tissue; 3 - muscle; 4 - skull; 5 - mandible; 6 - tongue; 7 - teeth; 8 - vertebrae; 9 - cartilage; 10 - thyroid gland; 11 - eyes; 12 - cerebrospinal fluid; 13 - cerebrum; 14 - cerebellum; 15 - brain stem; and 16 - pituitary gland

After designing the 3D head model, it was necessary to define the appropriate electromagnetic characteristics of each biological tissue and organ [26]. Biological tissues are non-homogeneous, non-linear, and dispersive, and each is defined by the corresponding electromagnetic quantities (permittivity, permeability, and conductivity). These parameters largely depend on the frequency, type of tissue, and its water content. In addition to these quantities, the density of the tissue for each tissue or organ is also required for a valid simulation.

2.2 Numerical Model of the 4G Helmet

Helmets must have a hard outer shell that absorbs impacts and is located around 2,5 cm above the head [27]. The shell is made from thermoplastics (polyethylene, polycarbonate, and others) and thermosetting materials (fiberglass and textile impregnated with phenol). These materials have proven to be durable, reliable, and lightweight, while providing effective protection [28]. The 4G smart helmet can also contain a range of additional devices and components, such as processors, displays, cameras, microphones, hard disks, power supply batteries, and communication modules [4, 12, 29]. One technical solution of the smart helmet is shown in Fig. 4.

The smart 4G helmet may have multiple antennas used for various purposes. It can contain a main antenna, an LTE diversity antenna, Wi-Fi and Bluetooth (BT) antennas, a GPS antenna, and a near-electric antenna. An example of a

PCB board with communication antennas is shown in Fig. 5.

Figure 4 A technical solution of the smart helmet [30]

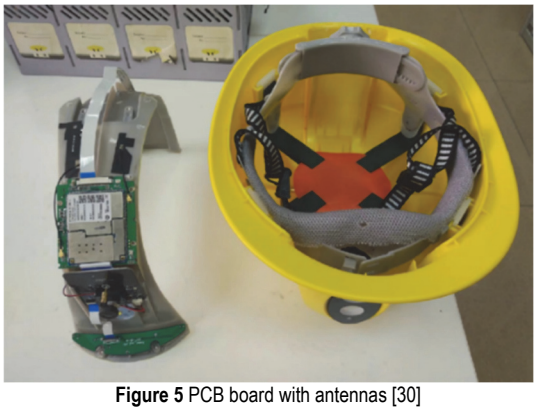

Figure 5 PCB board with antennas [30]

The 3D numerical model of the helmet created for this research corresponds to the actual dimensions and shape of the 4G helmet (Fig. 6). Likewise, the electromagnetic properties of the model helmet match those of a real-life 4G helmet [31-33].

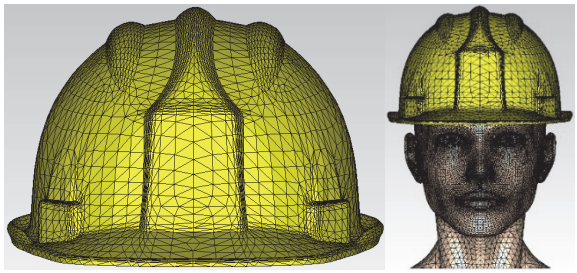

Figure 6 Numerical model of the helmet

The 4G smart helmet uses a 4G antenna [34] with 50 Ω impedance and 1 W power [35]. The S-parameters of the antenna are shown in Fig. 7.

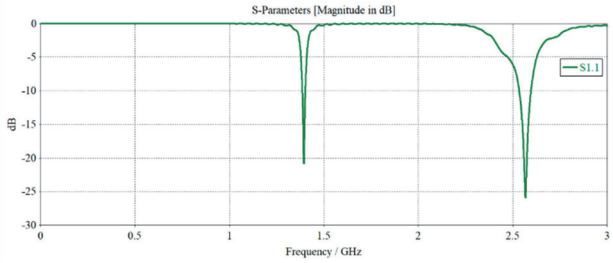

Figure 7 Reflection parameter of the 4G antenna

3 RESULTS

Based on the position of the antenna in the model, several vertical cross-sections were selected in which the analysis of the obtained values for electric field intensity and SAR_{1g} was performed. For each cross-section, one direction (C) was defined along which the electric field intensity and SAR are graphically displayed. The positions of the directions along which the assessment of the obtained results will be presented are shown in Fig. 8.

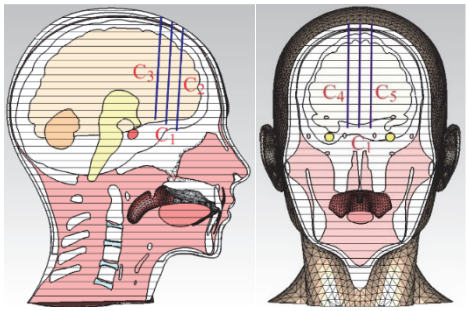

Figure 8 Positions of directions C_1, C_2, C_3, C_4, and C_5 within the numerical head model

The C_1 direction was chosen to be normal to the power supply of the antenna, while the other directions were set at equal distances relative to C_1 within each cross-section.

3.1 Analysis of Electric Field Intensity

Fig. 9 and Fig. 10 show the electric field intensity values on the models' surface with and without the helmet during communication via the 4G network. The areas on the surface of the helmet and the skin, shown in red in Fig. 9, represent regions with the highest electric field intensity exposure.

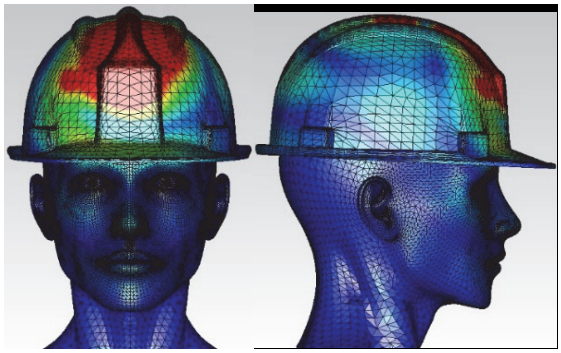

Figure 9 Helmet surface distribution of electric field intensity

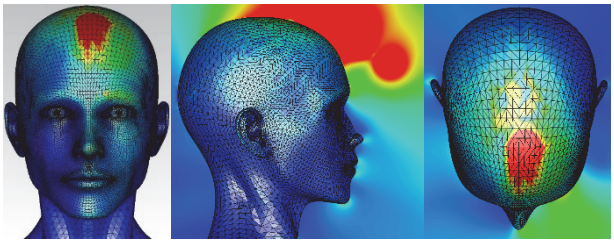

Figure 10 Head surface distribution of electric field intensity underneath the antenna

Figs. 11 to 13 show the electric field intensity inside the head model for horizontal cross-sections, where directions C_1, C_2, and C_3 are located, respectively.

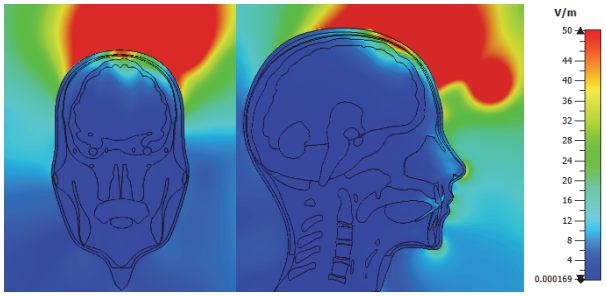

Figure 11 Electric field intensity - section with direction C_1 (two different planes)

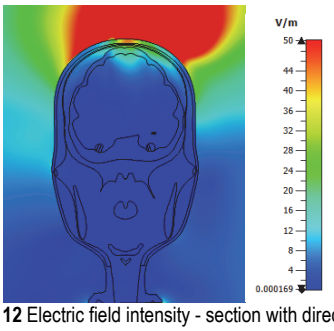

Figure 12 Electric field intensity - section with direction C_2

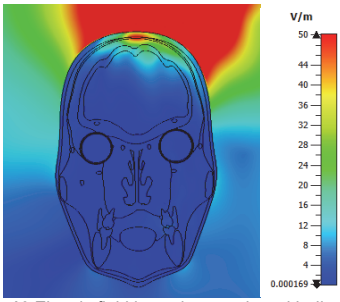

Figure 13 Electric field intensity - section with direction C_3

Fig. 14 and Fig. 15 show the electric field intensity distribution inside the head model for horizontal cross-sections where directions C_4 and C_5 lie, respectively.

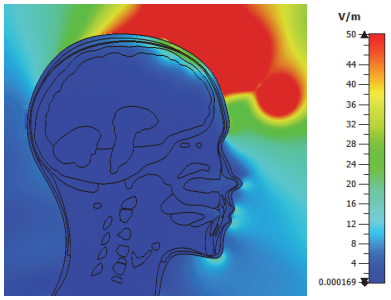

Figure 14 Electric field intensity - section with direction C_4

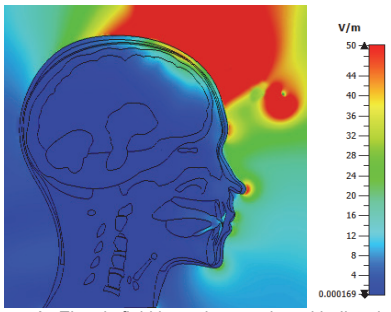

Figure 15 Electric field intensity - section with direction C_5

It is important to note that, for the sake of result clarity, the upper value of the electric field intensity is limited to 50 V/m in the color palette. Namely, the electric field is indeed the highest near the antenna and is significantly higher than in the head model. If the actual maximum field value were used in the color palette, the changes in the field value within the head would be almost invisible in the images. Since the changes within the head are the most critical for the analysis, it was necessary to adjust the graphical representation of the distribution of the quantities of interest. This means that the field values in areas shown in red may exceed the upper limit of the color palette.

According to the Regulation [22], the electric field reference limit at 2,6 GHz is 24,4 V/m in free space, without the presence of a human; however, figures show that the values in certain parts of the head model exceed this limit. The electric field intensity values and penetration depth of the electromagnetic wave, are indeed the highest in the area close to the antenna.

Fig. 16 and Fig. 17 show that electric field intensity is distance-dependent for the directions defined in Fig. 8.

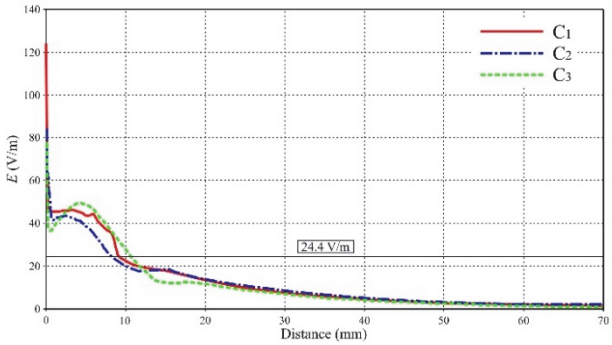

Figure 16 Variation of electric field intensity with distance in directions C_1, C_2, and C_3

The dependence of electric field intensity on distance along directions C_1, C_2, and C_3 is shown in Fig. 16. What is common to all three curves is that surface-layer electric field intensity in the head model significantly exceeds the reference limit levels. Electric field intensity for direction C_1 reaches its highest value of 125 V/m at the entrance to the head of the adult, and the field value drops below the reference limit at 9 mm from the start. It is evident that the penetration of the field is quite substantial, and high values extend through multiple tissues and organs. In that area of the head, the thickness of the skin, the adipose tissue, and the muscles is very small, so high values of electric field intensity are present even in the skull and the cerebrospinal fluid. The highest value is 32 V/m in the cerebrospinal fluid and 19 V/m in the brain. It needs to be noted that the regulation specifies field values in free space, without the presence of a human, and that these values in the body must be significantly lower as a result of absorption by the tissues and organs.

The highest value of electric field intensity along direction C_2 is 85 V/m, with a value of 24 V/m in the cerebrospinal fluid and 16 V/m in the brain. Elevated values above the reference limit are present up to about 8 mm. For direction C_3, values above the reference limit are present up to about 11 mm, with the highest value of electric field intensity being 78 V/m, while the highest values in the brain and the cerebrospinal fluid are 19 V/m.

Fig. 17 shows the graph of the variation of electric field intensity with distance in directions C_1, C_4, and C_5. Similar to the analysis of the graph in Fig. 16, the electric field

intensity values in the layers near the antenna for two directions - C_4 and C_5 - exceed the reference limit levels. For direction C_4, the value is 88 V/m at the entrance to the head of the adult, and it drops below the reference limit at 9 mm from the start. The highest value in the brain is 20 V/m. Along direction C_5, the highest value of electric field intensity is 37 V/m, 14 V/m in the cerebrospinal fluid and 12 V/m in the brain. The values above the reference limit are present up to about 8 mm.

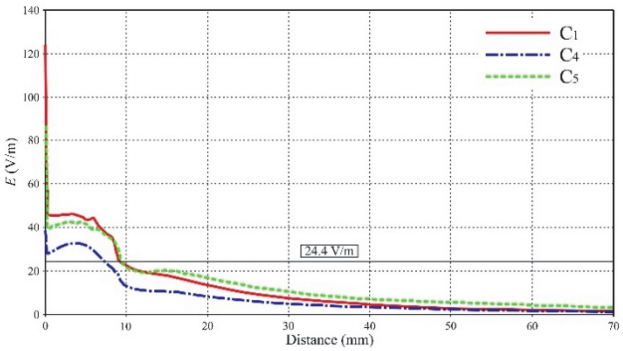

Figure 17 Variation of electric field intensity with distance in directions C_1, C_4, and C_5

3.2 Analysis of the Specific Absorption Rate

If a propagating electromagnetic wave encounters biological tissue, it penetrates that tissue allowing it to absorb some of its energy. The absorbed energy is precisely what is used to explain the impact of electromagnetic radiation on biological matter. For this purpose, a quantity called the Specific Absorption Rate was introduced. SAR is the rate at which energy from an electromagnetic wave is absorbed by human tissue per unit of mass, and this value can be provided as an averaged value over a specific mass of tissue or the entire body. A much more practical quantity is the averaged SAR, which is the ratio of power absorbed in the body to the mass of biological tissue. It is obtained by integrating the expression for local SAR over the entire desired volume. Calculation of averaged SAR usually involves a 1 g sample (SAR_{1g}) and a 10 g sample (SAR_{10g}). Because of thin layers in the model, with increased values underneath the antenna, it is more convenient to analyze the values of SAR_{1g}, as analyzing a final volume for SAR_{10g} would include multiple different tissues, making it impossible to determine the actual absorbed energy for just one tissue (one layer).

Fig. 18 shows the spatial distribution of SAR_{1g} and its maximum value at the head model surface. Figs. 19 to 23 show SAR_{1g} distribution within the head model for different cross-sections.

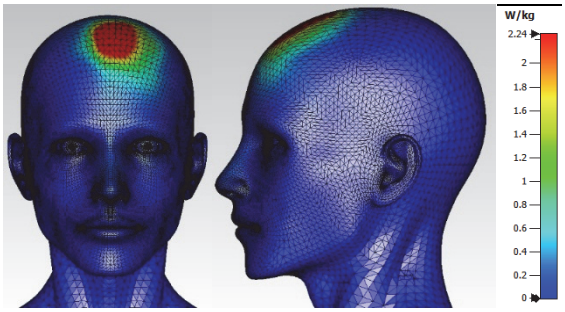

Figure 18 SAR_{1g} at the very surface of the model

It is evident from the figure that the maximum value for SAR_{1g} exceeds the basic limit of 1,6 W/kg [23].

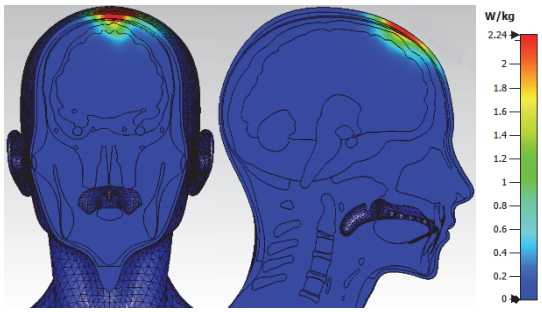

Figure 19 SAR_{1g} for the cross-section with direction C_1 (two different planes)

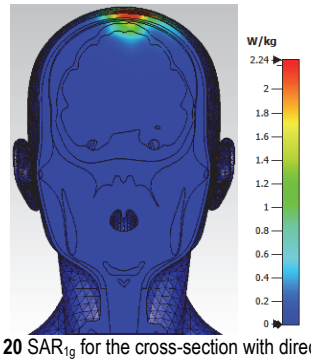

Figure 20 SAR_{1g} for the cross-section with direction C_2

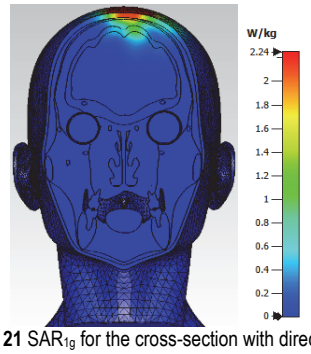

Figure 21 SAR_{1g} for the cross-section with direction C_3

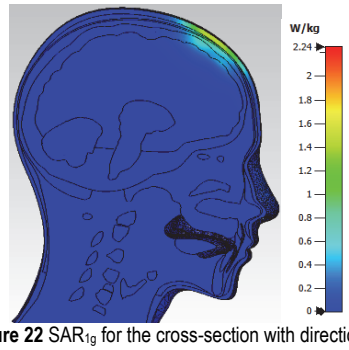

Figure 22 SAR_{1g} for the cross-section with direction C_4

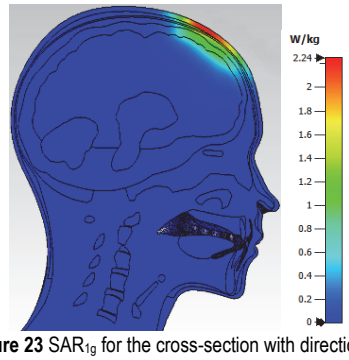

Figure 23 SAR_{1g} for the cross-section with direction C_5

From the figures, it is evident that the basic limits are exceeded in the surface layers, primarily in the skin, the adipose tissue, the muscles, and parts of the skull. Fig. 24 and Fig. 25 show the variation of SAR_{1g} values with distance for different cross-sections along directions C_1, C_2, C_3, C_4, and C_5.

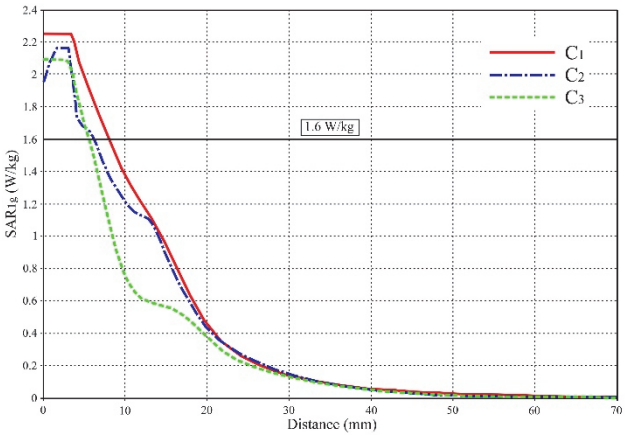

Figure 24 Variation of SAR_{1g} with distance in directions C_1, C_2, and C_3

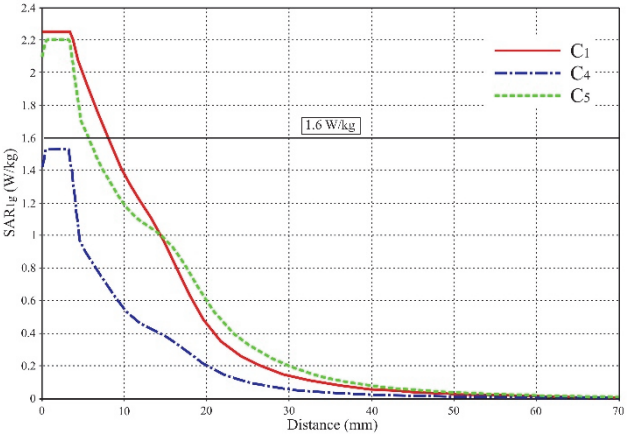

Figure 25 Variation of SAR_{1g} with distance in directions C_1, C_4, and C_5

The values for SAR_{1g} for each direction exceed the maximum allowed value of 1,6 W/kg (except in the case of distribution along direction C_4). For direction C_1, the maximum value for SAR_{1g} is 2,3 W/kg. Values above the basic limit are present up to a distance of 8,5 mm in multiple tissues, from the skin to the cerebrospinal fluid. In the cerebrospinal fluid, the highest value is 1,7 W/kg, while in the brain it is 1,2 W/kg.

For direction C_2, the maximum value for SAR_{1g} is 2,18 W/kg. Values above the basic limit are present up to a distance of 7 mm in multiple tissues, from the skin to the skull. The highest cerebrospinal fluid value is 1,6 W/kg, while in the brain it is 1,18 W/kg.

For direction C_3, the maximum value for SAR_{1g} is 2,1 W/kg. Values above the basic limit are present up to a distance of 6 mm, again in multiple tissues. The highest cerebrospinal fluid value is 1,1 W/kg, while in the brain it is 1 W/kg.

For direction C_4, the maximum value for SAR_{1g} is below the basic limit and amounts to 1,55 W/kg. Fig. 18 shows that higher values for SAR are more prominent on the left side of the numerical model of the head, but direction C_4 is in the cross-section outside that area. In the brain, SAR_{1g} is around 0,4 W/kg.

For direction C_5, the highest value is 2,2 W/kg. High values are present up to a distance of 6 mm in multiple tissues. In the brain, the highest value for SAR_{1g} is 0,9 W/kg.

For directions C_1, C_2, and C_3, the values for SAR_{1g} become the same at a distance of 30 mm, while from about 50 mm, they practically become negligible. For directions C_1, C_4, and C_5, the values for SAR_{1g} become the same at just over 50 mm, where they also become almost negligible and approach zero. For all directions beyond 70 mm, these values become almost equal to zero, indicating that at this depth there is almost complete absorption of electromagnetic energy.

4 CONCLUSION

This paper presented the results of a study on the effects of radiation emitted by a 4G smart helmet antenna within a numerical model that accurately represents the tissues and organs of the human head. For this purpose, two quantities were analyzed: the electric field and SAR, and the obtained values were compared with reference levels and basic limits. The antenna was set to operate at a frequency of 2,6 GHz. One way to make the work of employees safer and more efficient in specific industries is to connect protective helmets to wireless communication systems. Smart protective helmets can practically be viewed as hands-free wireless devices that can communicate with smartphones and computers via mobile networks. Since the 4G helmet is worn on the head, it was logical to assume that, due to the proximity of the helmet's antenna, the user's head would be continuously exposed to the EM field of the antenna.

For the numerical simulation, suitable 3D numerical models of the adult head, the helmet, and the 4G antenna were created. At the same time, all biological tissues and organs were represented by electromagnetic properties specific to them.

As a result of the 4G helmet antenna radiation simulation, the obtained values for the electric field and SAR within the numerical head model were analyzed. Since the antenna is located close to the head, it was expected that both electric field and SAR values would be high. After the obtained values for electric field intensity were analyzed, it was concluded that the reference values were exceeded by more than five times in certain tissues and organs. Namely, the exceedance of reference values for the different analyzed directions ranged from 1,3 to over 5 times, for electromagnetic wave penetration depths of 8 mm to 11 mm, depending on the direction. For the direction directly below the antenna feed, values higher than the reference values were present even in the brain.

The analysis of the distribution of SAR_{1g} showed that the basic limits were exceeded to a certain depth. These exceedances ranged from 1,3 to 1,4 times at depths ranging from 6 mm to 8,5 mm. Areas with greater absorption of electromagnetic energy include the muscles, the adipose tissue, the skin, the skull, the cerebrospinal fluid, and a small part of the brain. It was also evident that there are areas in the head model where both the electric field intensity and SAR values are extremely high and exceed several times the reference limit levels and basic limits. Particular attention should be paid to the tissues and organs

located in these areas in order to assess potential harmful biological effects. The values of the penetrated electromagnetic field would be much higher if the helmet shell rested directly on the user's head, that is, if there were no inlay located between the helmet shell and the head.

Even though the Smart Helmet was primarily designed as a powerful ally for employees to assist in their daily work, increase their safety, and enable a timely response in dangerous situations, the fact that it is an active source of electromagnetic radiation located directly above their heads must not be overlooked. Given that certain parts of the tissues and organs of the employees' heads are exposed to the electromagnetic field, special attention must be paid to the potentially harmful biological effects on the employees. Furthermore, it is necessary to examine the influence of the field on timely decision-making and reaction in certain situations, especially when employees are exposed to additional stress or work in difficult conditions.

New findings on the influence of electromagnetic field on Smart Helmet wearers can significantly contribute to the optimization of the Smart Helmet design and real-time exposure monitoring systems.

Future research will focus on other 4G frequencies, as well as 5G frequencies of mobile communication networks. Finally, all knowledge resulting from this and future studies can significantly contribute to the improvement of occupational safety and the adoption of adequate safety regulations.

Acknowledgements

This study was supported by the Ministry of Science, Technological Development and Innovation of the Republic of Serbia under the contract no.451-03-137/2025-03/200148; Goal 17.

5 REFERENCES

[1] Mertz, L. (2016). Are Wearables Safe?: We Carry Our Smart Devices with Us Everywhere - Even to Bed - But Have We Been Sleeping with the Enemy, or are Cautionary Tales Overinflated? *IEEE Pulse*, *7*(1), 39-43. https://doi.org/10.1109/mpul.2015.2498477

[2] Kim, S., Sharif, Y. A., & Nasim, I. (2024). Human electromagnetic field exposure in wearable communications systems: A review. *e-Prime - Advances in Electrical Engineering Electronics and Energy*, *8*, 100508. https://doi.org/10.1016/j.prime.2024.100508

[3] Kim, Y., & Choi, Y. (2022). Smart Helmet-Based Proximity Warning System to Improve Occupational Safety on the Road Using Image Sensor and Artificial Intelligence. *International Journal of Environmental Research and Public Health, 19*(23), 16312. https://doi.org/10.3390/ijerph192316312

[4] Jepower. (2025). *4G smart hard hat With Camera Live Streaming Camera For Construction*.

[5] Ouxiang international limited. (2025). *4G Smart Helmet Camera.*

[6] Choi, Y. & Kim, Y. (2021). Applications of Smart Helmet in Applied Sciences: A Systematic Review. *Applied Sciences*, *11*(11), 5039. https://doi.org/10.3390/app11115039

[7] Jayasree, V. & Kumari, M. N. (2020, July 23-24). *IOT based smart helmet for construction workers*. ICSSS, Chennai, India. https://doi.org/10.1109/icsss49621.2020.9202138

[8] Strasse, W. a. D., Campos, D. P., Mendonça, C. J. A., Soni, J. F., Mendes, J., & Nohama, P. (2022). Detecting bone lesions in the emergency room with medical infrared thermography. *BioMedical Engineering OnLine*, *21*(1). https://doi.org/10.1186/s12938-022-01005-7

[9] Campero-Jurado, I., Márquez-Sánchez, S., Quintanar-Gómez, J., Rodríguez, S., & Corchado, J. (2020). Smart Helmet 5.0 for industrial internet of things using artificial intelligence. *Sensors*, *20*(21), 6241. https://doi.org/10.3390/s20216241

[10] JOVE Video Communication Limited. (2025). *4G Smart Helmet*.

[11] Elefine. (2025). *Smart Safety Helmet with HD Camera Built-in Wifi 4G GPS SOS Positioning Live Video Network Camera*.

[12] Beijing Equiinet Network Technology Co., Ltd.(2025).*4G Smart Helmet EQ-M37*.

[13] Naobumi, M. & Hisashi, M. (2020). Helmet Antenna Design Using Characteristic Mode Analysis. *Applied Computational Electromagnetics Society Journal (ACES)*, *35*(2), 161-166.

[14] Michishita, N., Saita, Y., Morishita, H., Ameya, M., Hirose, M., & Kurokawa, S. (2020). Helmet-mounted inverted-F antenna at VHF band. *Journal of Advanced Simulation in Science and Engineering*, *7*(2), 291-299. https://doi.org/10.15748/jasse.7.291

[15] Gallucci, S., Bonato, M., Chiaramello, E., Fiocchi, S., Tognola, G., & Parazzini, M. (2022). Human exposure assessment to wearable antennas: Effect of position and interindividual anatomical variability. *International Journal of Environmental Research and Public Health*, *19*(10), 5877. https://doi.org/10.3390/ijerph19105877

[16] Nakao, T., Hung, N. T., Nagatoshi, M., & Morishita, H. (2012). Fundamental study on curved folded dipole antenna. *Proceedings of the 2012 IEEE International Symposium on Antennas and Propagation*, 1-2. https://doi.org/10.1109/APS.2012.6349370

[17] Wang, J. J. H. (2006). Broadband omnidirectional helmet antennas. *2006 IEEE Antennas and Propagation Society International Symposium*, 2129-2132. https://doi.org/10.1109/APS.2006.1711004

[18] Lee, A. K., Choi, H. D., Lee, H. S., & Pack, J. K. (2002). Human head size and SAR characteristics for handset exposure. *ETRI Journal*, *24*(2), 176-179. https://doi.org/10.4218/etrij.02.0202.0202

[19] Jovanovic, B. D., Stankovic, B. V., Cvetkovic, N. N., Krstic, D. D., & Vuckovic, D. (2019). The impact of human age on the amount of absorbed energy from mobile phone. *COMPEL - The International Journal for Computation and Mathematics in Electrical and Electronic Engineering*, *38*(5), 1465-1479. https://doi.org/10.1108/COMPEL-12-2018-0511

[20] CST Microwave Studio. (2012). *Version 2012.* Computer Simulation Technology.

[21] Mortazavi, S. M. J., Paknahad, M., Khaleghi, I., & Eghlidospour, M. (2018). Effect of radiofrequency electromagnetic fields (RF-EMFs) from mobile phones on nickel release from orthodontic brackets: An in vitro study. *International Orthodontics*, *16*(3), 562-570. https://doi.org/10.1016/j.ortho.2018.06.013

[22] Official Gazette of the RS. (2009). *Regulation on the limits of exposure to non-ionizing radiation*.

[23] IEEE. (2006). *IEEE Standard for safety levels with respect to human exposure to radio frequency electromagnetic fields, 3 kHz to 300 GHz* (Inc. C95.1-2005). https://doi.org/10.1109/IEEESTD.2006.99501

[24] Yee, K. S. (1966). Numerical solution of initial boundary value problems involving Maxwell's equations in isotropic media. *IEEE Transactions on Antennas and Propagation,14*, 302-307. https://doi.org/10.1109/TAP.1966.1138693

[25] Zygote Media Group, Inc.(2025). *ZygoteBody 3D Anatomy Online Visualizer*. zygotebody.com

[26] Hasgall, P. A., Di Gennaro, F., Baumgartner, C., Neufeld, E., Lloyd, B., Gosselin, M. C., Payne, D., Klingenböck, A., & Kuster, N. (2022). IT'IS database for thermal and electromagnetic parameters of biological tissues (Version 4.1). https://doi.org/10.13099/VIP21000-04-1
[27] OSHA. (2023). *Personal Protective Equipment*.
[28] Bullard. (2011). *Industrial Head Protection User Information Guide*.
[29] Global Sources. (n.d.). *Wireless Helmet Video Terminal*.
[30] BesoVideo Co. Ltd. (2021, January 26). *Kinds o fhelmet/hardhat 4G/5G/WiFi/GPS camera DVR, allin VMS/Smart Eye*.
[31] Sabet, M. & Soleimani, H. (2014). Mechanical and electrical properties of low density polyethylene filled with carbon nanotubes. *IOP Conference Series: Materials Science and Engineering*, *64*, 012001. https://doi.org/10.1088/1757-899X/64/1/012001
[32] Professional Plastics. (n.d.). *Electrical Properties of Plastic Materials*.
[33] Passador, F. R., de Faria, P. V., Backes, E. H. et al. (2017). Thermal, mechanical and electromagnetic properties of LLDPE/PANI composites. *Polymer Bulletin*, *74*, 2701-2717. https://doi.org/10.1007/s00289-016-1862-5
[34] Toro, J. & Choukiker, Y. K. (2017). Design and analysis of meander line PIFA antenna with MIMO system for mobile handheld device. *Proceedings of the 2017 International Conference on Trends in Electronics and Informatics (ICEI)*, 1061-1065. https://doi.org/10.1109/ICOEI.2017.8300872
[35] IEEE (2002), *C95.3-2002 - IEEE recommended practice for measurements and computations of radio frequency electromagnetic fields with respect to human exposure to such fields, 100kHz-300GHz*. https://doi.org/10.1109/IEEESTD.2002.94226

Contact information:

Vladimir STANKOVIĆ, PhD, Associate Professor
(Corresponding author)
University of Niš, Faculty of Occupational Safety,
Čarnojevića 10a, 18000 Niš, Serbia
E-mail: vladimir.stankovic@znrfak.ni.ac.rs

Dejan JOVANOVIĆ, PhD, Assistant Professor
University of Niš, Faculty of Electronic Engineering,
A. Medvedeva 14, 18000 Niš, Serbia
E-mail: dejan.jovanovic@elfak.ni.ac.rs

Anđela JEVTIĆ, PhD student, Research Trainee
University of Niš, Faculty of Occupational Safety,
Čarnojevića 10a, 18000 Niš, Serbia
E-mail: andjela.jevtic@znrfak.ni.ac.rs

Miomir RAOS, PhD, Full Professor
University of Niš, Faculty of Occupational Safety,
Čarnojevića 10a, 18000 Niš, Serbia
E-mail: miomir.raos@znrfak.ni.ac.rs

Dragana ŽIVALJEVIĆ, PhD, Assistant Professor
University of Niš, Faculty of Electronic Engineering,
A. Medvedeva 14, 18000 Niš, Serbia
E-mail: dragana.zivaljevic@elfak.ni.ac.rs